LBL--16695

DE84 008248

DEVELOPMENT OF NEUTRON-TRANSMUTATION-DOPED GERMANIUM BOLOMETER MATERIAL

Nicholas Paul Palaio
(M.S. Thesis)

Lawrence Berkeley Laboratory
University of California
Berkeley, California 94720

August 1983

This work was supported in part by NASA Contract No. W-14,606 under Interagency Agreement with the Director's Office of Energy Research, Office of Health and Environmental Research, U.S. Department of Energy under Contract Number DE-AC03-76SF00098.

ABSTRACT

The behavior of lattice defects generated as a result of the neutron-transmutation-doping of germanium was studied as a function of annealing conditions using deep level transient spectroscopy (DLTS) and mobility measurements. DLTS and variable temperature Hall effect were also used to measure the activation of dopant impurities formed during the transmutation process. In addition, a semi-automated method of attaching wires on to small chips of germanium (< 1 mm^3) for the fabrication of infrared detecting bolometers was developed. Finally, several different types of junction field effect transistors were tested for noise at room and low temperature (~ 80 K) in order to find the optimum device available for first stage electronics in the bolometer signal amplification circuit.

ACKNOWLEDGMENTS

I would like to thank my advisor, Dr. Eugen Haller, for his support and guidance throughout the course of my project. I am especially grateful to Dr. Steven Pearton for his invaluable assistance and guidance offered during the defect annealing study. I also acknowledge the assistance and advice given by my fellow lab partners, and technical staff: Dick Davis, Paul Luke, Robert McMurray, Nancy Haegel, William Hansen, Blair Jarrett, Marilyn Rodder, Jack Walton, and Heinrich Sommer. Last but not least, a final thanks to Michelle Bailey, Vicki Donelson, Kazuo Shimada, and Lynne Dorey for their help in preparing this thesis.

This work was supported in part by NASA Contract No. W-14,606 under Interagency Agreement with the Director's Office of Energy Research, Office of Health and Environmental Research, U.S. Department of Energy under Contract No. DE-AC03-76SF00098.

TABLE OF CONTENTS

I. INTRODUCTION

Bolometers belong to a general class of thermal detectors used to measure infrared radiation. The basic component of all thermal detectors is a sensing element with a bulk physical property which exhibits a temperature dependence. When radiation is absorbed, the temperature of the sensor rises and the change in the temperature sensitive property and thus radiation is measured. This operation may be contrasted with a photoconductor, where the signal is generated not by a temperature fluctuation but by discrete carrier excitation and collection processes. Many different temperature sensitive properties have been used to monitor radiation: gas pressure, dielectric constant, liquid volume, pyroelectric effect, etc. The bolometer uses the temperature dependence of electrical resistivity as its basis of operation. The first bolometer was developed by Langely[1] in 1880 and consisted of a resistor made of platinum wire. Different metals with higher temperature coefficients of resistance were substituted as the need for more sensitive bolometers for more sophisticated applications became necessary. During World War II, Bell Laboratories developed the first semiconducting bolometer. Because the resistivity of semiconductors is exponentially dependent on temperature as opposed to the linear dependence of metals, and because of the wealth of knowledge and processing expertise brought about by the solid state electronics revolution, semiconductors quickly replaced metals as the optimum bolometer material. Today bolometers are used at room temperature as burglar and fire alarms and at cryogenic temperatures in IR astronomy and spectroscopy experiments. For example, cryogenically cooled semiconducting bolometers are currently being used to measure the diffuse

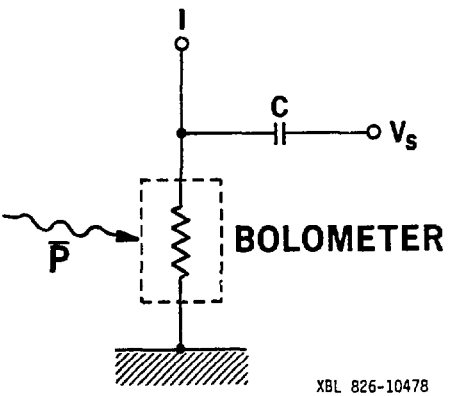

Figure 1. Bolometer electrical circuit.

background radiation of the universe believed to be a remnant of the Big Bang.[2] In contrast to bolometers, photoconductors are used with excellent results to study select portions of the infrared spectrum. But since the signal from a photoconductor originates from direct carrier excitations from specific energy levels in the bandgap rather than by a bulk physical property (as in the case of bolometers), their response starts abruptly at a given wavelength and extends over a relatively limited frequency range. The longest wavelengths (~ 200 μm) have been detected using stressed gallium doped germanium photoconductors. Bolometers, which detect all the absorbed power are inherently broad band going to long wavelengths (< 1000 μm). Using bolometers, researchers have discovered the spectrum of the cosmic background radiation to closely resemble that of a 3 K black body.

The electrical circuit for a bolometer is shown in figure 1. In the dark, a constant current through the detector causes a measurable

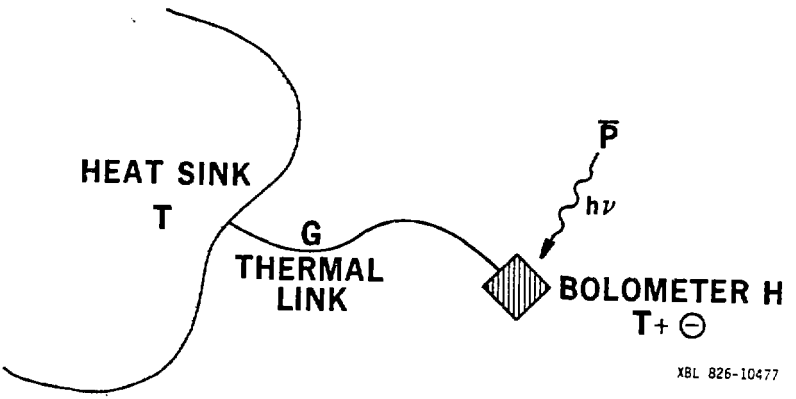

Figure 2. Schematic of bolometer thermal equivalent circuit.

voltage drop across the bolometer resistance. When exposed to radiation, however, the bolometer heats up, causing a change in its resistance and a change in the voltage drop across the device. This measured voltage change is the bolometer output signal, V_s. Since the bolometer is a thermal detector it has a thermal circuit analogous to its electrical circuit. Referring to figure 2, the bolometer is connected to a heat sink by a thermal link, G (usually the electrical leads), and in the dark remains at a constant temperature, T, equal to that of the sink. When pulsed with radiation, the detector's temperature rises by an amount θ. The dynamics of heat transfer to the sink and thus the "speed" of the device are governed by the thermal time constant, $\tau = H/G$, where H is the bolometer thermal mass. A detailed analysis of bolometer operation is given in the appendix.

The fundamental sensitivity limit of a bolometer is restricted by

the noise sources inherent to the operation of this type of thermal detector. The two sources of noise which impose the fundamental detection limit of a bolometer are the Johnson noise associated with thermally induced random charge motion in the resistive element and the thermal conductance noise associated with random phonon fluctuations through the thermal link. These two terms are generally described in sum as the noise equivalent power (NEP) which is defined as the incident power required to generate a voltage output from the device equal to the noise measured in a 1 Hz bandwidth,

$$(NEP)^2 = \frac{4kTR}{S^2} + 4kT^2G$$

where T = temperature, R = bolometer resistance, S = bolometer responsivity, G = thermal conductance, and k = Boltzmann's constant. From this expression it can be easily seen that the fundamental sensitivity of the device may be increased by decreasing the operating temperature. In addition, lowering the operating temperature lowers the heat capacity of the device[3] thus increasing the responsivity. These reasons combined with the demand from the astrophysics community for devices with lower NEP led to the development of cryogenic bolometers. The first cryogenic bolometer design used the strong temperature dependence of resistivity at the superconducting transition of a metal film as its basis of operation.[4] The problems associated with operation of this type of bolometer, temperature control within 10^{-5} K and poor radiation absorption, led the search for alternate materials and modes of operation. As a result, the emphasis has shifted to the use of semiconductors as the resistive elements. The first liquid helium cooled semiconducting bolometer was developed by Low[5] in

1961, using highly doped and highly compensated germanium. Development of germanium bolometers continued with a drive to lower operating temperatures (0.1 K) and improved construction techniques. Richards and co-workers[6] introduced a composite bolometer consisting of the germanium resistor soldered to a bismuth-coated sapphire substrate which acts as a radiation absorbing antenna. Recently, interest has been shown in using silicon as an alternative to germanium as the resistive element. Approaching absolute zero, the heat capacity of pure silicon is lower than germanium due to its lower Debye temperature.[7] At low temperatures, the heat capacity of both silicon and germanium is dominated by lattice vibration; however, the high doping levels required for low temperature bolometers adds an additional electronic component to the heat capacity. This electronic component arises from delocalization of impurity electrons or holes when high doping levels result in substantial wave function overlap.[8] This complexity has led to considerable debate in the detector community as to which material, silicon or germanium, is the preferred on the basis of heat capacity. Silicon bolometers have been successfully developed by Chanin[9] and Kinch.[10] In a novel design, Downey[11] used the planar technonogy of the microelectronics industry to construct an integrated, ion implanted silicon bolometer.

The following sections describe the continuing development of neutron-transmutation-doped germanium for low temperature bolometers, as well as low noise electronics for bolometer signal amplification. Discussed initially is the neutron-transmutation-doping of germanium and the results of an annealing study into neutron irradiation induced defects. Next, a method of soldering electrical leads on to small

germanium chips (0.5 x 0.5 x 0.3 mm^3) for the fabrication of bolometers is presented. Finally, the requirements of a low noise amplification system, including the room and low temperature noise testing of junction field effect transistors for first stage bolometer electronics are discussed.

II. NEUTRON-TRANSMUTATION-DOPING AND DEFECT ANNEALING OF GERMANIUM

A. Neutron-Transmutation-Doping of Germanium.

The requirement that the material used for bolometers has a resistivity that is a strong function of temperature makes doped, single crystal semiconductors the most widely used material. Traditionally, this material is fabricated by adding dopant impurities to the melt prior to Czochralski crystal growth. The incorporation of dopants in this manner presents some fundamental problems when applied to optimizing the material for bolometers.

The distribution of impurities in the Czochralski crystal is defined by the effective segregation coefficient and the impurity concentration in the melt. In general, impurity atoms have a higher concentration in the liquid phase that in the adjacent solid; therefore, as the crystal is pulled, impurity atoms are continually rejected into the melt, leading to a positive compositional gradient from head to tail of the crystal. A well known exception to this rule is boron in germanium with a segregation coefficient less than one. Superimposed on this macroscopic segregation are local compositional fluctuations resulting from the dynamics of crystal growth. Oscillations in growth rate, non-planar solidification front, and convective stirring of the melt all lead to longitudinal and radial inhomogeneities on the micron to millimeter scale.[12]

The electrical conduction mechanism at low temperatures (< 10 K) which defines the bolometer resistance is a strong function of both the net dopant concentration ($|N_A - N_D|$) and the compensation ratio of minority to majority dopants (N_A/N_D for an n-type semiconductor). In the case of an n-type semiconductor, at these low

temperatures, very few electrons are promoted to the conduction band and thus are able to carry current. Instead, conduction is accomplished amongst impurities by the tunneling of electrons from an occupied donor to a donor which has been left unoccupied due to compensation, as shown in figure 3. Since the tunneling probability is exponentially dependent on the distance between occupied and unoccupied sites, it follows that the macroscopic conductivity is greatly dependent on the concentration of majority dopants as well as the compensation.[13] It is precisely for this reason that melt doped semiconductors with their inherent dopant inhomogeneities, make it extremely difficult and time consuming to select a crystal section possessing the correct doping condition leading to an optimum bolometer resistance for a particular application. As mentioned previously, one alternative to melt doping has been proposed by Downey[11] in the form of an ion implanted Si:As

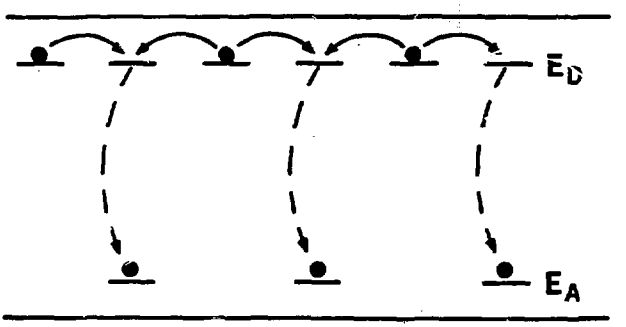

XBL 836-10207

Figure 3. Hopping conduction in an n-type semiconductor.

TABLE I. NTD REACTIONS FOR GERMANIUM.

Isotope Fraction	Reaction	Cross Section (b)	$t_{1/2}$
20.5	$^{70}_{32}Ge(n,\gamma)\ ^{71}_{32}Ge \rightarrow\ ^{71}_{32}Ga + K$	3.25	11.2d
27.4	$^{72}_{32}Ge(n,\gamma)\ ^{73}_{32}Ge$	1.0	stable
7.8	$^{73}_{32}Ge(n,\gamma)\ ^{74}_{32}Ge$	15.0	stable
36.5	$^{74}_{32}Ge(n,\gamma)\ ^{75}_{32}Ge \rightarrow\ ^{75}_{33}As + \beta^-$	0.52	82.8m
7.8	$^{76}_{32}Ge(n,\gamma)\ ^{77}_{32}Ge \rightarrow\ ^{77}_{33}As + \beta^- \rightarrow\ ^{77}_{34}Se + \beta^-$	0.16	11.3d

monolithic bolometer. Although this method offers the convenience in processing provided by the well developed planar IC technology, the yield of useful devices is less than 20% due to resistivity inhomogeneities of bolometers implanted with identical schedules. Clearly a reliable and reproducible method of producing a quantity of material which will yield a large number of identical bolometers is needed.

A solution to this problem of dopant and resistivity inhomogeneity can be found in neutron-transmutation-doping (NTD). NTD silicon has been used commercially for about one decade in high voltage rectifiers and thyristors where uniform dopant distributions are essential for smooth breakdown characteristics.[14] Similarly, this well established neutron irradiation technology may be applied to germanium for use as low temperature bolometer material. When germanium is exposed to a flux of thermal neutrons (E ~ 25 meV), the five naturally occurring isotopes partake in capture and decay reactions as shown in Table I. The isotopes of interest are ^{70}Ge, ^{74}Ge, and ^{76}Ge since their decay yields gallium, arsenic, and selenium -- all of which are

electrically active impurities in substitutional positions in the germanium lattice. The gallium acceptors are produced in excess of the sum of the arsenic donors and selenium double donors in a constant compensation ratio:

$$K = \frac{N_{As} + 2N_{Se}}{N_{Ga}} = 0.322$$

defined by the relative abundance and capture cross-section of their parent isotopes. Most importantly, since the parent isotopes are distributed uniformly, in a random fashion throughout the crystal, the resulting impurities are also uniformly distributed. Since the number of dopants formed is simply the product of isotopic concentration, neutron capture cross-section, and neutron fluence, the net dopant concentration may be controlled over a wide range by varying the total neutron dose. Thus, the two most critical parameters influencing low temperature conduction in bolometers -- impurity concentration and compensation -- are entirely controllable and uniform throughout the material.

The capture cross-section, when multiplied by the isotopic concentration defines the probability of neutron capture and thus the eventual number of impurity atoms produced. In general, the capture cross-section, σ_c, is related to the energy of the incident neutron by

$$\sigma_c \sim E^{-\frac{1}{2}}$$

for neutron energies up to $\sim 10^4$ eV. Not all the germanium isotopes of importance follow this dependence accurately which makes it difficult to directly compare or predict results obtained in

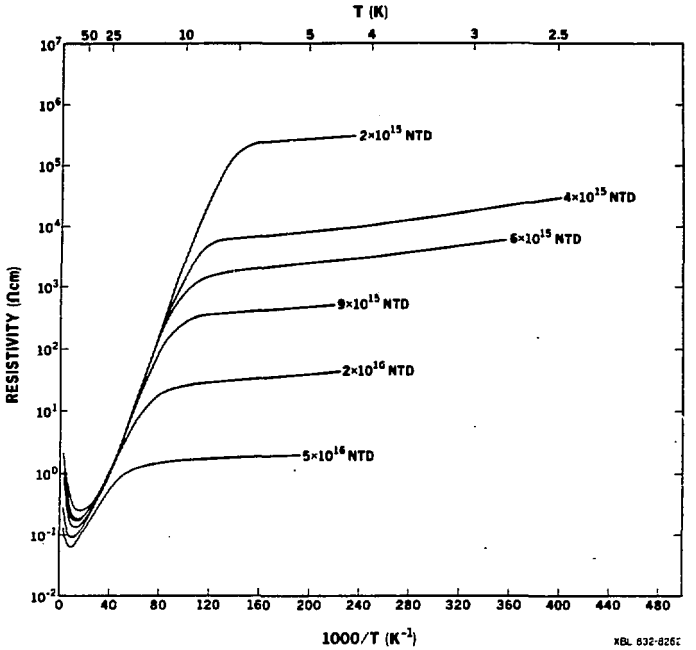

Figure 4. Low temperature resistivity of NTD germanium with Ga concentrations of 2 x 10^{15} – 5 x 10^{16} cm.$^{-3}$.

different reactors. For further improvement of this situation, work in regard to accurate determination of $\sigma_c(E)$ is needed, though this should be considered as a secondary effect.

As a portion of previous thesis work,[15] six slices of ultra-high purity germanium ($|N_A - N_D| < 10^{11}$ cm^{-3}) were irradiated with neutrons to gallium concentrations of 2 x 10^{15} to 5 x 10^{16} cm^{-3}. The resistivity of these samples was measured to low temperatures (0.3 K) and found to follow the following empirical relationship in the low temperature regime (T < 8 K):

$$\rho = \rho_0 \exp(\Delta/T)$$

where ρ = resistivity, ρ_0 = exponential prefactor, T = temperature, and Δ = exponential argument related to the temperature coefficient of resistance. As can be seen from figure 4, the resistivity in the low temperature "hopping" conduction regime described previously is extremely sensitive to majority dopant concentration. An increase in gallium concentration of slightly more than an order of magnitude results in a decrease in resistivity of almost 6 orders of magnitude.

B. Defect Generation in NTD Semiconductors.

It is well known that the NTD process generates structural damage within the semiconductor single crystal. There are two main sources of this damage. The foremost cause is direct knock-on displacement of atoms by high energy fast neutrons which do not contribute in the transmutation reaction, but inevitably accompany the thermal neutron flux. The second major cause is due to atom recoil upon thermal neutron capture or particle emmission during transmutation. Although no information is available as to the nature of this damage in germanium, quite a bit of work has been done involving NTD silicon. A model proposed by Stein[16] describes defect areas existing as high density clusters at the endpoint and along the path traversed by the fast neutron or recoiling atom. Electron paramagnetic resonance studies have revealed complicated point defects including multi-vacancy and interstitial clusters, as well as vacancy or interstital-impurity (primarily oxygen and phosphorus) complexes.[17] In most cases, the density of these defects tends to be almost two orders of magnitude lower than that calculated. Results of Raman spectroscopy have shown that the majority of the displacement energy appears to be dissipated by creating highly disordered, perhaps amorphous material which do not appear

as point defects.[17]

The presence of the structural damage resulting from NTD has been proven to be detrimental to the electrical properties of the irradiated material. Decreases in carrier mobility and minority carrier lifetime, as well as the generation of deep levels in the bandgap which act as free carrier traps, have all been substantiated through a variety of electrical measurements in NTD silicon.[17] In addition, dopant impurities formed during transmutation will tend not to be located in their usual electrically active substitutional positions, although they may contribute a carrier as a result of a shallow level formed in conjunction with a point defect. Thermal annealing is the most commonly used method for repairing neutron damage and activating dopants. Again, many studies have been made with regard to NTD silicon. It is generally agreed upon that annealing at 750°C for 30 minutes is sufficient to remove virtually all detectable neutron radiation damage in silicon and restore carrier concentration and mobility to predicted values.[18] Minority carrier lifetime is the only electrical parameter which does not exhibit full recovery, remaining lowered at even higher annealing temperatures.

To our knowledge, only one study involving the annealing behavior of NTD germanium is known to have been conducted. Kuriyama and coworkers[19] irradiated n-type ($N_D = 5.9 \times 10^{13}$ cm^{-3}) germanium with a neutron dose of 1.8×10^{15} cm^{-2} and performed a series of isochronal anneals for thirty minutes at 100°C increments from 100 - 600°C. Room temperature Hall effect measurements showed radiation damage resulting in a number of shallow acceptors ten times in excess of the calculated net acceptor concentration. Thermal annealing at

increasing temperatures decreased the carrier concentration toward the calculated value and increased the free carrier mobility. Rutherford backscattering channeling experiments confirmed the existance and recovery of neutron damage in annealed material when compared with non-irradiated starting material. No detail, however, was given concerning the behavior of specific defects under different annealing conditions. Therefore, it is aim of this portion of the thesis to present results which spectroscopically distinguish electrically active point defects and confirm their annihilation during thermal and recombination enhanced annealing.

C. Deep Level Transient Spectroscopy.

The most effective technique used to identify the presence of deep levels in semiconductors is deep level transient spectroscopy (DLTS).[20] In DLTS, a diode fabricated out of the material of interest is reverse biased. The bias is periodically reduced to allow filling of shallow and deep levels in the depletion region with majority carriers. When the bias is returned to its quiescent value, the carriers are emitted from the filled levels at a rate that is a strong function of temperature and energy of the level. This filling and emptying process, as a function of diode voltage, is shown in figure 5 for an n^+-p junction. In this case, holes are the majority carriers which are alternately captured and emitted from shallow acceptors and deep hole traps in the depletion region. The emission rate of a carrier from a level can be expressed in the following manner:[20]

$$e = \frac{\sigma N \langle v \rangle}{g} \exp(-E_T/kT)$$

e = emmission rate of carrier from the deep level to the nearest band

σ = deep level free carrier capture cross-section

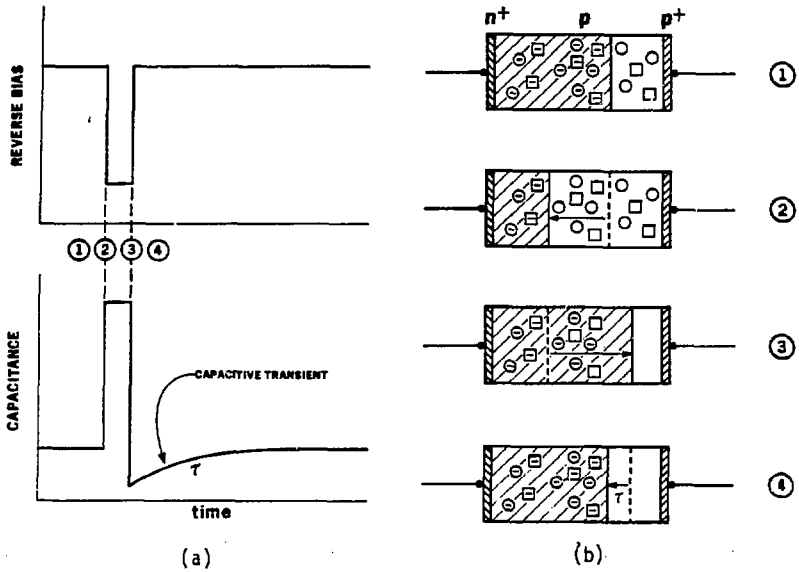

Figure 5. (a) Time dependence of bias and of capacitance of a partially depleted p-n semiconductor junction in a Deep Level Transient spectrometer. (b) Change of the depletion layer and the charge state of shallow (circles) and deep (squares) acceptors in a p-i-n device.

N = density of states in the valence or conduction band
$\langle v \rangle$ = carrier average thermal velocity
g = degeneracy of level (usually taken to equal 2)
E_T = trap energy level measured from the appropriate bandedge
k = Boltzmann's constant
T = temperature

This expression may be simplified by consolidating the first few terms and considering their temperature dependences:

$$e = AT^2 \exp(-E_T/kT)$$

An experimental temperature range is chosen so that the emission from shallow levels is almost instantaneous, while the emission from deep levels is accomplished with a measurable time constant, $\tau = 1/e$. The emission transient may be detected by measuring the time dependent

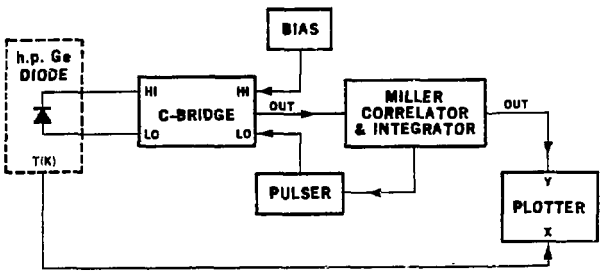

Figure 6. Block diagram of simple Deep Level Transient Spectrometer.

capacitance of the diode during pulsing and is shown in the period 3 to 4 in figure 5. The capacitance transient may be processed in a variety of ways. A technique developed by Miller[21] was used in this experiment. The output signal of a 1 MHz capacitance bridge placed across the diode is multiplied by an exponentially decaying reference waveform of chosen time constant, then integrated using the Miller correlator as shown in figure 6. When the time constants of the capacitance bridge and reference waveform are equal, the output of the correlator reaches a maximum. This matching of time constants will occur at a specific temperature depending on trap energy as indicated in the above equation. Pulsing is performed over a wide temperature range so traps of all energies will have an emission rate at some temperature corresponding to the reference signal. Traps will appear as local maxima (peaks) in the plot of correlator output versus temperature. This plot is the DLTS spectrum. Minority carrier traps may also be detected by pulsing into forward bias or by creating minority

carriers using bandedge light. The resulting correlator output appears as local minima when emission and reference time constants are equal.

Changing the time constant of the reference waveform will correspondingly change the temperature at which it equals the emission time constant, and thus displaces the maxima of the correlator output with respect to temperature. If a number of spectra are run with different time constants, an Arrhenius plot of τT^2 versus 1/T (where T is the temperature of the DLTS peak) will yield a slope corresponding to the deep level activation energy and a y-intercept related to the capture cross-section of the level. DLTS may also be used to determine the acceptor/donor nature of the trap by observation of the Poole-Frenkel effect. The high electric field across the p-n junction (10^4 - 10^5 V/cm) lowers the coulombic binding energy between a bound hole and its acceptor ion (p-type) or a bound electron and its donor ion (n-type).[22] Thus, the emission rate of a carrier given in the previous equation may be modified to include this field enhanced effect,

$$e = AT^2 \exp \frac{-E_T + \Delta E}{kT}$$

where ΔE is the barrier reduction given by,

$$\Delta E = q\left(\frac{qE}{\pi\epsilon}\right)^{\frac{1}{2}}$$

$$= 1.9 \times 10^{-4} qE^{\frac{1}{2}} \text{ eV for germanium}$$

where q = electronic charge, ϵ = dielectric constant of germanium, and E = average electric field. By varying the magnitude of the pulse reductions, the average electric field across the diode and the corresponding carrier emission rate will change. This causes a

measurable shift in the DLTS peak with respect to temperature. For defects which exhibit the Poole-Frenkel effect, an Arrhenius plot of $E_T - \Delta E$ versus $E^{\frac{1}{2}}$ will produce a slope equal to $1.9 \times 10^{-4} q$ eV/(V/cm)$^{\frac{1}{2}}$, the Poole-Frenkel constant for germanium. Majority carrier traps exhibiting this behavior may be determined to be acceptors in p-type semiconductors or donors in n-type semiconductors.

D. Recombination Enhanced Annealing of Deep Levels.

Thermal annealing has been the traditional method of annealing radiation and ion implantation damage in semiconductors. The activation energy necessary to repair structural damage is met by heating the crystal to a sufficiently high temperature at which the material is held for a time sufficient to annihilate the defects present. Motivated by possible contamination of the material by impurities in the furnace and undesirable migration of impurities in diffused or implanted areas, there has recently been an effort to find alternatives to high temperature--long duration thermal annealing. Laser, flash lamp, and graphite strip heater annealing of extremely short duration have all been developed to confine a high temperature cycle to the outer surface.

In the experiment to be described, recombination enhanced annealing (sometimes called injection annealing) has been used alone or in conjuction with low temperature thermal annealing. Recombination enhanced annealing uses the energy released upon electron-hole recombination to anneal defects present in the crystal. In a forward biased diode, electrons injected into the p-type region recombine with holes at a distance within the diffusion length from the junction. Often

this recombination occurs at a defect acting as deep trap. In this case, the recombination energy $E_C - E_T$ is transfered to the lattice at the defect site and annealing is accomplished on a highly localized level. If the annealing rates of thermally annealed and injection annealed material are compared as a function of temperature, the activation energy for thermal annealing is closely correlated to the sum of the activation energy for injection annealing plus the recombination energy. Recombination enhanced annealing has been used in repairing radiation damage in GaAs and GaP,[23,24] and has recently been observed in electron and γ-irradiated Ge.[25,26]

E. Experimental Work.

Ultra-high purity germanium grown at the crystal growth facility at the Lawrence Berkeley Laboratory was used as starting material for neutron-transmutation-doping. This material is ideally suited for NTD since the concentration of residual, electrically active impurities is extremely low (10^{10} -10^{11} cm^{-3}) compared to the resulting doping levels. Neutral impurities, carbon, oxygen, hydrogen, and silicon, are also present in amounts up to 10^{14} cm^{-3}. Only silicon partakes in a neutron transmutation reaction, yielding one phosphorus atom for every 10^{11} gallium atoms produced. One 4 cm diameter, 5 mm thick slice of ultra-high purity germanium was irradiated with a neutron dose of 1 x 10^{17} cm^{-2} at the University of Missouri Research Reactor.[27] After storage for eight months at room temperature, the material was sawed into 5 x 5 x 3 mm^3 samples and etched in the standard 3:1 (HNO_3:HF) solution. Isochronal thermal annealing at 300, 400, and 500°C for one hour was performed in a quartz tube under flowing argon gas. Isothermal thermal annealing at 400°C for 0.25,

0.5, 1, 2, 4, and 6 hours was also performed under the same furnace conditions. After annealing, the 77 K Hall mobility of each sample was measured using the Van der Pauw method.[28] These same samples were next prepared for DLTS by diffusing an n^+ lithium contact (5 minutes at 280°C) on to one 5 x 5 mm^2 face to form a diode, and rubbing InGa eutectic on the opposite face to form a p^+ ohmic contact. DLTS was conducted using the experimental set-up described in the introduction and shown in figure 6. Several annealed and unannealed diodes were forward biased over a range of currents and temperatures in the DLTS system to study the occurrence of recombination enhanced annealing. In addition, variable temperature Hall effect was performed down to 10 K on an unannealed sample using a continuous flow liquid helium cryostat to study the activation of dopants.

F. Discussion of Results.

Figure 7 shows several DLTS spectra taken under a variety of thermal annealing conditions. The lack of prominent hole traps in the unannealed sample spectrum is a result of highly disordered regions within the crystal. This result agrees with information presented earlier concerning NTD silicon. Most of the displacement energy has been dissipated in forming large cluster defects which are not detectable using DLTS. Annealing at 300°C for one hour is sufficient to repair these regions, leaving several hole traps clearly visible as peaks on the given spectra. The activation energies of the hole traps were determined from the Arrhenius plots in figure 8 and are listed along with their capture cross-sections in Table II. Hole traps H(0.10), H(0.22), and H(0.37) exhibit the Poole-Frenkel effect and have thus been determined to be acceptors. As shown in figure 9, the

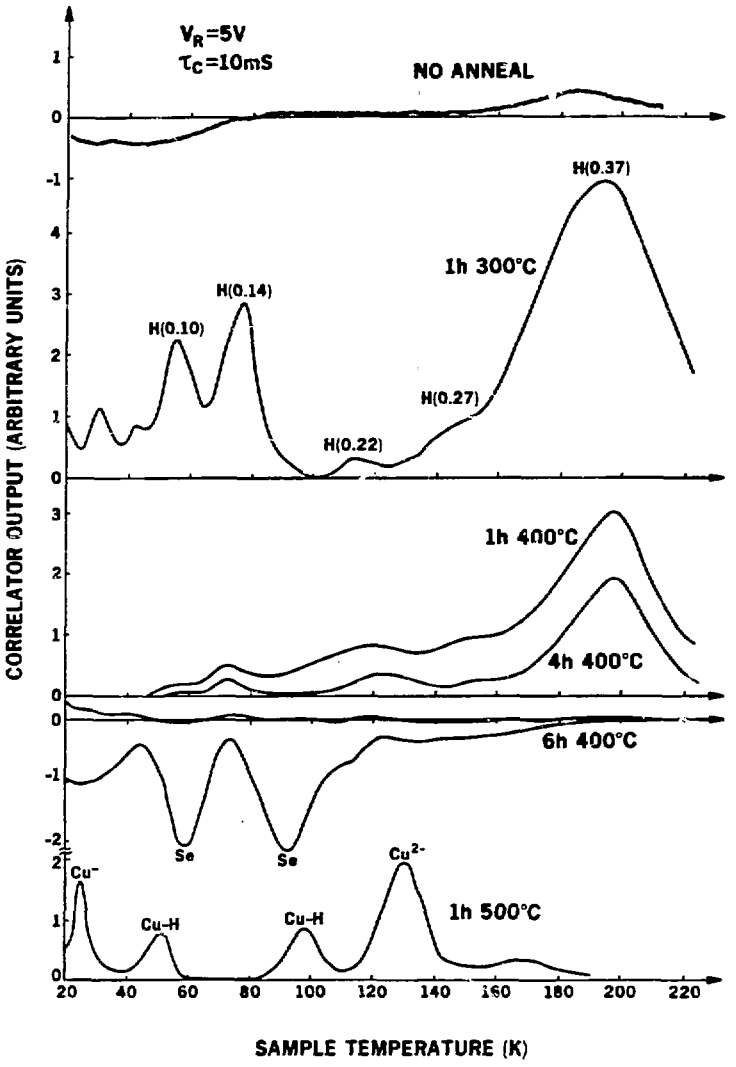

XBL 837-10724

Figure 7. DLTS spectra as a function of annealing time and temperature.

DLTS spectra for two of the defects displays peak shifting with electric field as the bias reduction is increased from 1 to 9 volts. From this peak shifting, the field dependent activation energy ($E_T - \Delta E$) of the traps can be plotted versus the square root of the average electric field as in figure 10 to yield a slope of 1.8×10^{-4}q eV/$(V/cm)^{\frac{1}{2}}$ for H(0.37) and 2.0×10^{-4}q eV/$(V/cm)^{\frac{1}{2}}$ for H(0.22). Both values are in good agreement with the value of 1.9×10^{-4} eV/$(V/cm)^{\frac{1}{2}}$ derived from the simple model formulated by Frenkel.[29] The activation energies listed in Table II for levels exhibiting Poole-Frenkel shifting are the extrapolated zero field values.

Defect peak heights are diminished with increasing annealing temperature and time until complete annihilation of the deep levels, within the sensitivity of DLTS ($\sim 10^{11}$ cm^{-3}), is realized by annealing at 400°C for 6 hours. Although annealing at 500°C for only one hour appears to reduce NTD related defects substantially, the sample becomes contaminated with rapidly diffusing copper. The 500°C spectrum shows the several well known Cu related deep levels detected. The suppression of copper contamination of germanium has been noted by Hall[30] as a result of a pre-anneal soaking of the germanium crystal in potassium cyanide. Repair of lattice damage is further confirmed by measurements of 77 K Hall mobility as a function of annealing time at 400°C and shown in figure 11. The substantial increase in hole mobility realized after just 15 minutes at 400°C most likely corresponds to the repair of the highly damaged regions previously mentioned. Annealing for longer times brings about a saturation of the mobility to a value of ~7400 V/cm^2sec, indicating repair of crystalline damage is approaching completion.

TABLE II.

Designation	Energy (eV)	Hole Capture Cross-section (cm^2)	Comment
H(0.10)	E_v + 0.10	1.7×10^{-16}	acceptor
H(0.14)	E_v + 0.14	3.4×10^{-15}	
H(0.22)	E_v + 0.22	3.0×10^{-17}	acceptor
H(0.27)	E_v + 0.27	10^{-17} est.	
H(0.37)	E_v + 0.37	3.7×10^{-17}	acceptor

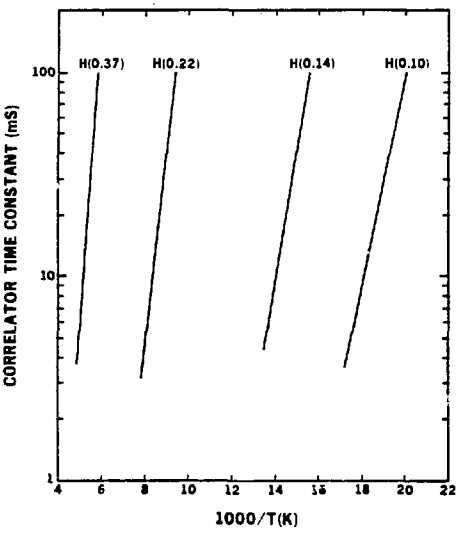

Figure 8. Arrhenius plots of hole traps from which cross sections and energies were determined.

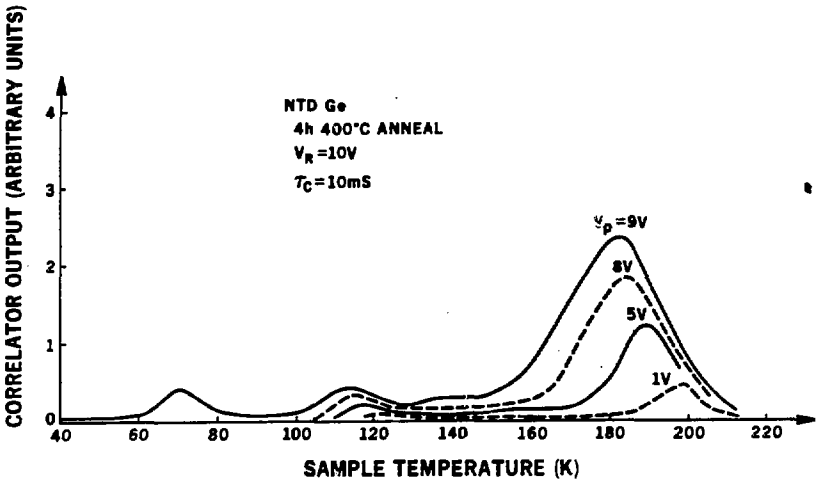

Figure 9. DLTS spectra of NTD Ge showing Poole-Frenkel defect peak shifting as the average electric field in the depletion region is increased.

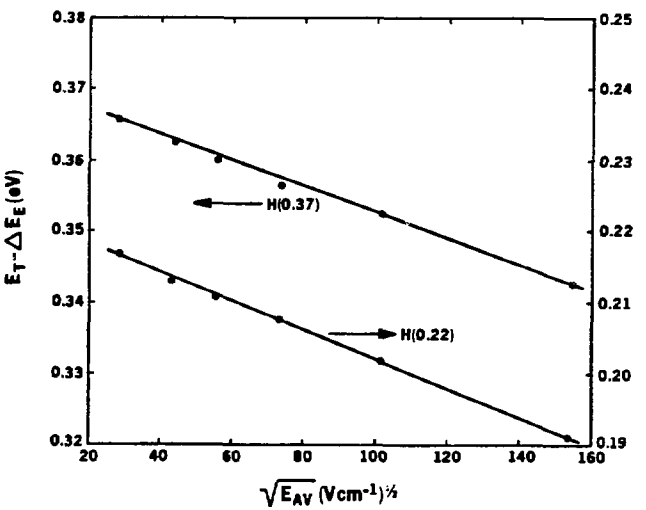

Figure 10. Dependence of apparent energy level position of two hole traps as a function of average electric field, labelled by their extrapolated zero field energies.

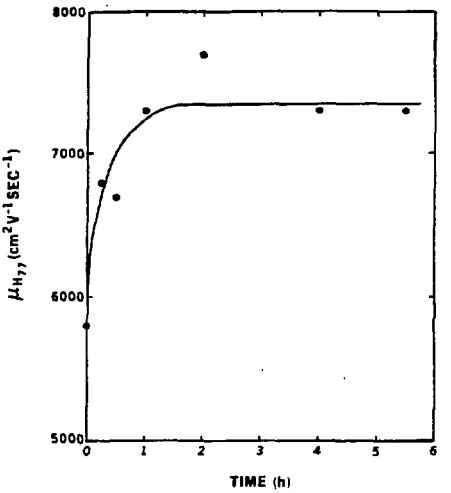

Figure 11. Variation of 77 K Hall mobility with annealing time at 400°C.

Another interesting feature apparent in the 400°C, 6 hour spectrum are the negative peaks associated with minority carrier traps detected during forward biasing pulsing. These peaks correspond to the two ionization states (E_C - 0.14 and E_C - 0.28 eV) of the deep selenium double donor generated during neutron-transmutation-doping. Due to the displacement of recoiling germanium isotopes during neutron capture and ß decay, it is generally thought that only a small fraction of the dopants formed occupy electrically active substitutional positions in unannealed material. From DLTS spectra, the relative selenium concentration as a function of annealing temperature is plotted in figure 12. Complete activation corresponds to 5.6 x 10^{13} cm^{-3} calculated from the neutron fluence and isotope cross-section. This result shows the success of thermal annealing in activating dopant

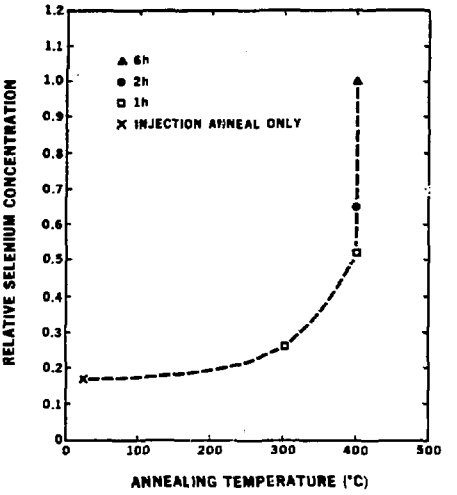

Figure 12. Variation of relative Se concentration with annealing temperature and time.

impurities, as well as in repairing lattice damage.

As mentioned, it has been assumed that few of the gallium, arsenic, and selenium occupy electrically active substitutional positions immediately after irradiation. Figure 13 shows a plot of free carrier concentration as a function of inverse temperature generated by variable temperature Hall effect measurements made on an unannealed sample. The two slopes of the freeze-out curve represent the full (11 meV) and half (5.5 meV) activation energies of shallow acceptors, such as gallium, in germanium. The change in slope corresponds to the presence of compensating arsenic and selenium donors created by NTD. The concentration of compensating donors can be estimated by the half slope to full slope transition point and is equal to 5×10^{14} cm^{-3}. Comparing this value to the calculated value of $N_{As} + 2N_{Se}$ equal to

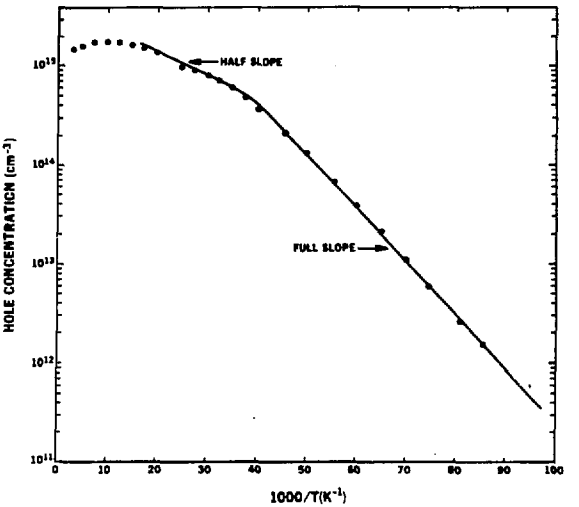

Figure 13. Variable temperature Hall effect freeze out curve showing the half to full slope freeze out transition of shallow acceptors.

1×10^{15} cm^{-3}, it is interesting to note that approximately one half of the donors have been activated without thermal annealing. It is not known whether this activation is realized immediately after irradiation or as a result of room temperature storage for 8 months, but the result is noteworthy considering the heavily damaged nature of the material.

The effects of recombination enhanced annealing on the stability of defects was also studied. An unannealed sample was treated with a series of 3.0 A/cm^2 injections at room temperature. A DLTS spectrum was taken after each treatment to chart the progress of defect annealing. These spectra are shown in figure 14. As was noted in the

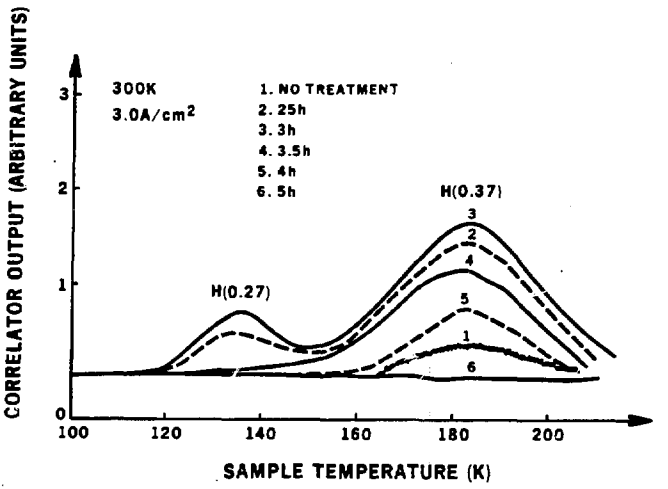

Figure 14. DLTS spectra showing the recombination enhanced annealing of deep levels in unannealed material at increasing injection times.

thermal annealing study, the unannealed sample provided only one weak peak due to the dominance of extensive cluster damage. As this damage is reduced by injection annealing for longer times, two point defect trapping levels, H(0.27) and H(0.37), become more evident. The low concentration of hole traps during the initial stages of injection annealing (< 3 hours) is an artifact of the disordered regions present in the depleted region. Once there is significant annealing of these regions, the concentration of hole traps is shown to be reduced by recombination of electrons and holes at defects in the vicinity of the junction. The effectiveness of recombination enhanced annealing is further confirmed by the comparison of annealing activation energies of injection and thermally annealed samples. The DLTS spectra of a

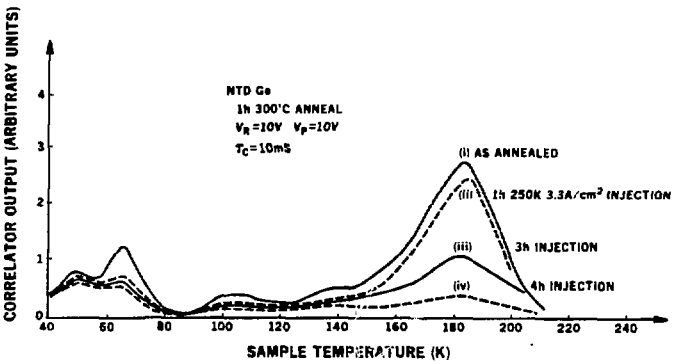

Figure 15. DLTS spectra from NTD Ge annealed at 300°C for one hour, then subject to an injected current density of 3.3 A/cm^2 for various periods.

sample thermally annealed at 300°C for one hour and then subsequently injection annealed for several one hour periods at 3.3 A/cm^2 is shown in figure 15. From the change in concentration of the deep level with injection time, the annealing rate was determined. This process was repeated at several different current densities and the annealing rate calculated for each. Using this data, the annealing rate of the H(0.37) defect was plotted in figure 16, as a function of injection current density, revealing 2.5 A/cm^2 as the saturation current. Using a current density of 3.0 A/cm^2, the annealing rate of the H(0.37) level was measured at 250, 270, and 290 K. Figure 17 compares the annealing rate as a function of annealing temperature of these injection annealed samples with samples previously thermally annealed. The slope of each straight line gives the activation energy of annealing. The activation energy for the thermally annealed samples was calculated to be 0.65 eV while that for the injection

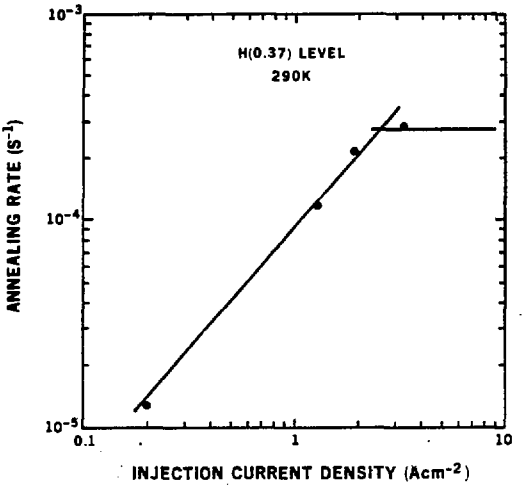

Figure 16. Annealing rate of the H(0.37) acceptor level as a function of injection current density.

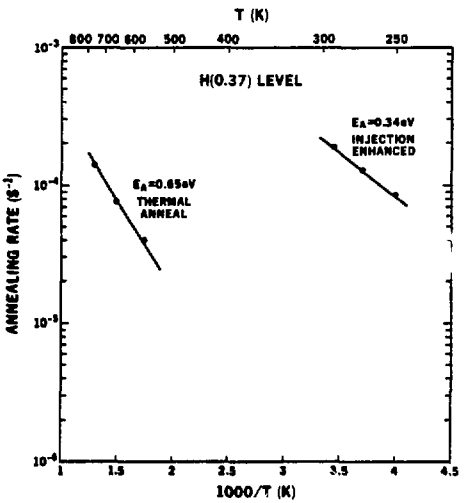

Figure 17. Comparison of annealing rate of the H(0.37) acceptor with temperature for thermal and injection annealing.

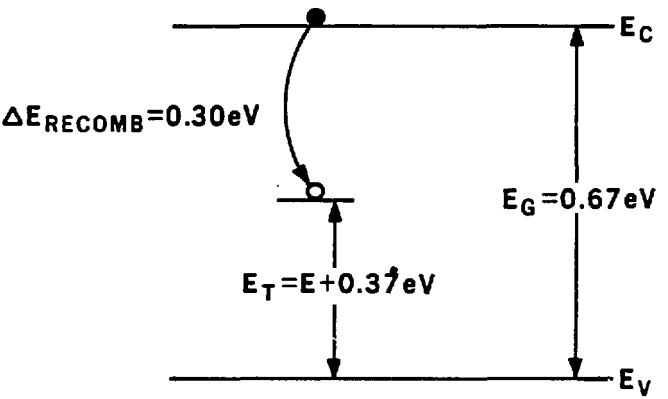

Figure 18. Energy band diagram showing electron-hole recombination at a deep trap and the resulting energy released.

annealed was 0.34 eV, corresponding to energy released by an electron during recombination from the conduction band to the E_V + 0.37 eV deep level. This recombination is shown in figure 18.

Since the diffusion length of electrons in our material is on the order of a millimeter, the effectiveness of recombination enhanced annealing should be confined to within this distance of the junction. As a further check that the disappearance of the levels was due to recombination enhanced annealing, ~1.5 mm of material was removed from an injection annealed sample, and the remaining piece recontacted. DLTS measurements on the newly contacted sample confirmed the presence of each of the five deep levels previously detected.

G. Discussion of Defect Models.

The microstructure of the deep levels induced by the NTD process is unclear. The levels found in NTD germanium are likely to be vacancy

related, and may indeed be due to multi-vacancy clusters. It is the general consensus[31,32,33] that in germanium, radiation induced defects are vacancy related as opposed to interstitial related. Interstitials formed during irradiation have high mobility and even at room temperature can recombine with the surface, dislocations, and some vacancies, leaving a large vacancy related defect concentration behind.[34] In contrast, lower mobility vacancies can remain as electrically active multi-vacancy complexes or in conjunction with impurity atoms. Evidence of impurity-vacancy complexes has been found in room temperature γ-irradiated experiments.[35] Arsenic-vacancy complexes produce a hole trap at E_v + 0.10 eV which matches our H(0.10) level measured by DLTS. It is reasonable to assume that one or more of the remaining levels may be attributed to vacancy pairings with gallium and selenium produced as a result of transmutation. The residual electrically active impurities in the ultra-high purity germanium starting material (P, Al, B) are present in concentrations of ~10^{10} cm^{-3} which is two orders of magnitude below the concentration of defects measured (~ 10^{13} cm^{-3}). Thus, complexes of these impurities with lattice damage cannot be responsible for the levels observed. Also present in the high purity starting material are the electrically neutral impurities, hydrogen, oxygen, and silicon, in concentration of approximately 10^{14} cm^{-3}. In high purity material similar to that used in this study, fast neutron irradiations at much lower doses (10^{9} cm^{-2}) produced complexes of these impurities with radiation induced lattice defects.[36] However, in the more heavily irradiated NTD material, the transmutation products and lattice damage are expected to dominate the resultant defect spectrum. Thus, it is not

surprising that neutral impurity-defect complexes were not observed in NTD germanium.

In conclusion, deep levels generated in the germanium crystal during neutron-transmutation-doping are most likely associated with multi-vacancy and transmutation impurity-vacancy complexes. Thermal annealing provides the energy necessary for defect dissociation and trap annihilation. Recombination enhanced annealing at room temperature is effective by concentrating the electron-hole recombination energy at the defect site, thus altering the lattice configuration at the defect and eliminating the deep level. The amount of energy released upon recombination at level H(0.37), for example, has been shown to be 0.30 eV. Relating the energy to an equivalent temperature with Boltzmann's constant gives

$$T \sim E/k = 3300\ K$$

Thus the localized deposition of this relatively large amount of energy (compared to thermal annealing) can be appreciated as an extremely efficient method of annealing defects.

III. BOLOMETER FABRICATION

As mentioned in the introduction, the sensitivity of a bolometer may be increased by minimizing its thermal mass. Often this requirement results in extremely small detectors (a cube with sides < 0.5 mm, for instance), thus making electrical lead attachment a difficulty. The lack of hand coordination and steadiness makes it virtually impossible to handle soldering iron, wire (often as thin as 1 mil), and detector while making a bond which will survive the stresses induced when cooling to liquid helium temperatures.

It was soon realized that to attach leads to a 0.5 x 0.5 x 0.3 mm^3 germanium chip would require designing a semi-automated process. This process, beginning with the germanium chip preparation, will now be discussed. A 0.3 mm thick germanium wafer was initially prepared by ion implanting the faces to be contacted to high concentrations of boron.[37] This process yields degenerate p^{++} contacts on the p-type germanium. When doped to such high concentrations (~ 10^{20} cm^{-3}), the contacts are metallic and exhibit ohmic behavior down to the lowest temperatures. Next, two metal layers, first 500 Å of titanium then 8000 Å of gold, were sputtered on to the contact faces. Gold is used since it makes a superior solder bond as compared to a plain germanium surface. Titanium functions as a cementing layer and as a diffusion barrier as gold adheres poorly to germanium and may form a eutectic during annealing. The wafer is annealed at 200°C for 30 minutes to relieve residual stresses in the metal films. The wafer, ion implanted and metallized on opposite sides, is diced in grid fashion using a wire saw to yield a large number of 0.5 x 0.5 x 0.3 mm^3 chips. These chips are ready for electrical lead attachment. An apparatus

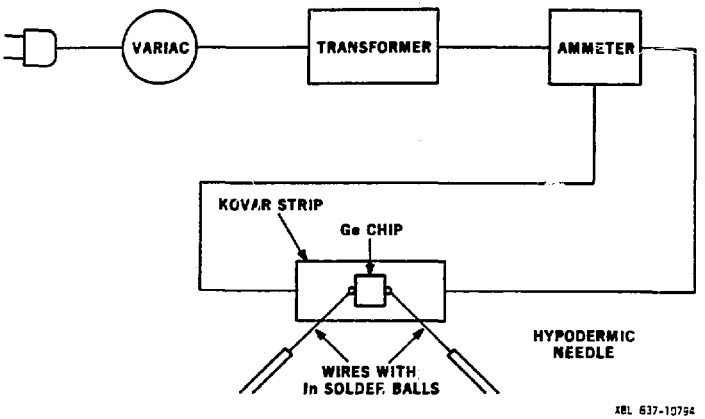

Figure 19. Schematic diagram of bolometer wire attachment apparatus.

was designed and constructed to allow wire attachment with a minimum amount of chip handling and operator attention. Shown in figure 19, the chip is positioned on a thin strip of Kovar which acts as a heating element when current from the variable power supply is passed. Each wire (3 mil dia., 1 cm long copper) for attachment is held in the hollow shaft of a hypodermic needle which has in turn been clamped into the jaws of a micro-manipulator. The ends of the wires have been previously tinned with ~ 0.2 mm diameter balls of indium solder, coated with a thin layer of rosin flux. With the aid of a microscope positioned above, the wires are guided to opposite sides of the chip so that the fluxed indium solder balls are just touching the 0.5 x 0.5 mm^2 metallized contact areas. With chip and wires positioned correctly, the bonds are now ready to be made. A slowly increasing current is passed through the Kovar strip until the flux is observed to melt and wet the metallization. As the current is increased further (to ~ 7 A),

the indium melts (157°C) and begins to alloy with the gold. The power supply is then turned off, the indium solidifies within a fraction of a second, and the bond is made. The wires are carefully removed from the hypodermic needles with tweezers which is also a good test of bond quality.

Bonding in this fashion leaves the germanium surface contaminated with solder flux and dirt from the Kovar strip, as well as roughened from wire sawing and positioning on the Kovar. Thus the chip must be given a post-bond etch. The standard 3:1 (nitric to hydroflouric acid) etch used for germanium is also quick to dissolve the copper wires. Therefore, the wires are thoroughly coated with Picene wax and the device, now a bolometer, is etched for one minute. After etching, the wax may be easily removed using trichloroethylene.

Owing to the many problems encountered along the way, the development of this contacting method was accomplished in a trial-and-error fashion. For example, the addition of flux to the indium solder balls came after it was realized that the surface of the indium oxidizes quickly upon heating, creating a gummy oxide sheath which renders the wire unsolderable. Also, the yield of useful devices was lowered due to adherence problems at the germanium-titanium interface. After wire sawing, the metallization would flake off of up to 50% of the chips, with more failures at each handling step. Out of improvements made in contact metallization of nuclear radiation detectors,[38] it was discovered that a 200 Å electron-beam evaporated layer of palladium in substitution of titanium forms an intermetallic compound of palladium and germanium at the interface during stress relief annealing. Analogously, metal-silicides have been used extensively in the IC industry

for low barrier ohmic contacts and Schottky barriers. In our case, the germanium-palladium-gold scheme proved superior with metallization adhesion of 100% of the chips after wire sawing. All of our future bolometers will be constructed using this metallization procedure.

IV. CONSTRUCTION OF LIQUID HELIUM CRYOSTAT AND LOW NOISE AMPLIFICATION SYSTEM

A. Electronics Requirements of Bolometer Circuits.

The ultimate performance of bolometers like any other detector producing an electrical signal is often limited by the amount of electrical noise inherent to the detector and its amplification system. When the power incident from the radiation source is high, the electrical noise present in the detector output signal is dominated by the statistical random arrival of photons upon the detector. When the power incident from the radiation source is low, however, the noise can be dominated by the detector and its amplification system. It has already been shown that noise in the detector may be reduced by operation at lower temperatures, thus reducing Johnson and thermal conductance noise. Current dependent excess noise arising in the electrical contacts to the detector has been substantially reduced by using heavily doped, ion implanted contacts described in the section on bolometer fabrication. The low noise operation limit of a bolometer will not be realized, however, if noise from the bolometer signal amplification system is overwhelming. Therefore, it is extremely important to choose the lowest noise amplifiers available. Often this process involves extensive testing of different devices until the optimum device is found. Such a procedure is discussed later in this section.

Major sources of extraneous noise in bolometer systems are voltage fluctuations resulting from mechanical vibrations in the cryostat, in the bolometer, and along the long wires which carry the bolometer signal from the device to the first stage electronics. An equivalent bolometer circuit including bias current I, a parallel combination of load resistance and bolometer resistance R_{eff}, bolometer

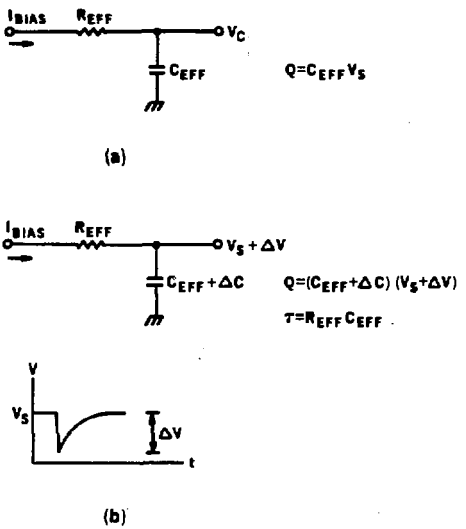

Figure 20. (a) Equivalent steady-state bolometer circuit. (b) Equivalent bolometer circuit after a small displacement in the signal carrying wire and the resulting voltage transient.

signal voltage V_s, and combined bolometer, load resistor, and signal wire capacitance C_{eff}, is shown in figure 20. In the steady state, there is a voltage V_s across the capacitor corresponding to a total charge of $Q = C_{eff}V_s$. Any small physical displacement of the signal wire relative to ground will cause a fluctuation ΔC in the effective capacitance which results in a ΔV added to the bolometer signal voltage. ΔV returns to zero with a time constant, $R_{eff}C_{eff}$, as charge is added or removed from the capacitor. The magnitude of ΔV may be reduced by reducing ΔC (e.g. by shortening the signal wire). The shortening of the high impedence signal wire has several advantages. Vibrations in a shorter wire will be smaller in amplitude and shorter in

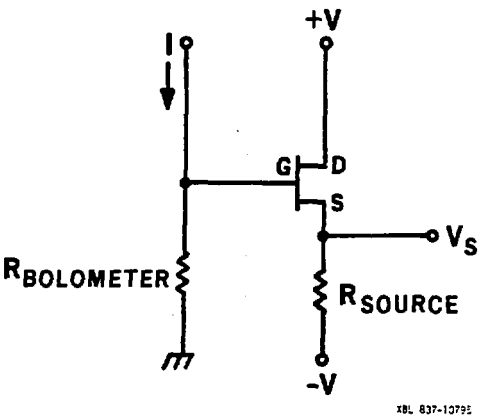

Figure 21. Bolometer circuit including JFET source follower pre amplifier. The source, gate, and drain of the JFET are referred as S, G, and D, respectively. R_{source} is a transistor biasing resistor while +V and -V are transistor power supplies. The signal voltage is taken from the source and is equal to the gate voltage plus a constant gate-source offset.

duration. In addition vibrations will be higher in frequency thus moving the interfering effects to higher frequencies outside the signal frequency range. A shorter signal wire also reduces voltage pickups from adjacent wires and stray fields. The duration of ΔV or the time constant may be reduced by decreasing the output resistance, R_{eff}. Typically, bolometers have a high load resistance of 1 to 20 MΩ since noise from the best amplifiers are minimized with source resistances in this range and the bolometer responsivity is directly proportional to its resistance. A proven way to shorten the high R_{eff} wire from the bolometer and to reduce the output resistance seen by the long wires carrying signal from the cryostat is to station a first stage amplifier in the form of a source follower junction field effect transistor in close proximity to the bolometer. Shown

in figure 21, a similar concept has been used successfully in photoconductor applications.[39] Since the FET is located in an ambient of 4.2 K or below and is inoperative (due to carrier freeze-out) below ~ 55 K, the transistor must be enclosed in an insulating housing with a heater resistor to keep it at an operating temperature.

B. JFET Source Follower and Noise.

FET source followers are commonly used as unity gain amplifiers when impedence lowering is desired. The term source follower is used because the voltage measured at the source remains equal to the signal voltage fed into the gate plus a constant gate-to-source offset voltage. The gain of the amplifier is

$$A = \frac{g_m R_s}{1 + g_m R_s}$$

where g_m is the transconductance of the device and R_s is the source biasing resistor. When $R_s >> g_m^{-1}$, the gain of the amplifier is close to one. Most importantly, the output impedence is equal to g_m^{-1} which is on the order of a kΩ.

It must be kept in mind that the noise from each device in the bolometer detector system must be minimized to attain the lowest possible NEP. JFETs are especially well suited to this task because they exhibit low noise even with high source resistances as is the case with bolometers. The noise in an FET may be separated into two components: voltage noise and current noise. The voltage noise represents the Johnson noise of the FET channel and can be expressed by[40]

$$e_n = \sqrt{4kT(0.67/g_m)B}$$

where k = Boltzmann's constant = 8.62×10^{-5} eV/K, T = temperature (K), B = frequency bandwidth (Hz). In addition, at low frequencies, the voltage noise contains a second term which describes an excess noise component proportional to f^{-n}. In this case the expression for e_N is

$$e_N = \sqrt{4kT(0.67/g_m)B(1 + f_1/f^{-n})}$$

where f_1 is the "knee" of the 1/f region (100 Hz to 1 kHz) and n is a constant between one and two. The 1/f region is of special interest for bolometer circuits since many applications require signal chopping frequencies below 10 Hz. The severity of 1/f noise is controlled to an extent through design; however, it has been recognized that there is a close link to device processing since it varies from lot to lot of the same device. The second component of noise in an FET is the current noise which is caused by the thermally generated reverse leakage current across the gate-channel reversed bias junction. The current noise may be expressed as

$$i_N = \sqrt{2qI_gB}$$

where q = charge of the electron and I_g = leakage current across the reverse biased junction. For the frequencies at which bolometers are used the current noise may be considered constant with frequency and may be added in quadrature to the voltage noise to get a total noise voltage of

$$e_{N_{total}}^2 = e_N^2 + i_N^2 R_{eff}^2$$

The best JFETs available today have room temperature current noise values of well below 10^{-15} A/$\sqrt{Hz}$ and even lower values at reduced

operating temperatures. Thus in our R_{eff} range, the noise from the FET shall be dominated by the voltage noise term.

The experimental work in the next section describes the process of selecting an FET on the basis of lowest voltage noise at low frequencies (< 10 Hz) for use as a first stage amplifier as described above. Also considered along with the selection process is both the construction of a housing to insulate the FET from its < 4.2 K ambient and the design and construction of a liquid helium experimental cryostat.

C. Cryostat Construction.

The initial step toward performing low temperature experiments was the construction of a liquid helium cryostat. There are several types of cryostats available commercially, but for reasons of versatility it was decided an immersion construction following a design used for many years in the Berkeley Physics department would be utilized.[41] Constructed was an insert consisting of a 2 in. diameter, 3 in. long cylindrical sample chamber suspended from a top plate by 4 stainless steel tubes (3/8 in. dia., 10 mil wall, 3 ft. long) which also acted as a vacuum line (one) and a housing for electrical leads (three). Also mounted on the top plate was a stainless steel light pipe for possible optical experiments and a heavy walled stainless steel tube for liquid helium transfer. The sample chamber shown in figure 22 consisted of an extension of the light pipe on which a detector may be mounted, a silicon optical window, and a flat base to be used to mount electronics. Vacuum tight seals (< 10^{-6} Torr at room temperature) were made around the circumference of the can with a deformable indium seal, at the silicon window using Stycast low temperature epoxy,[42]

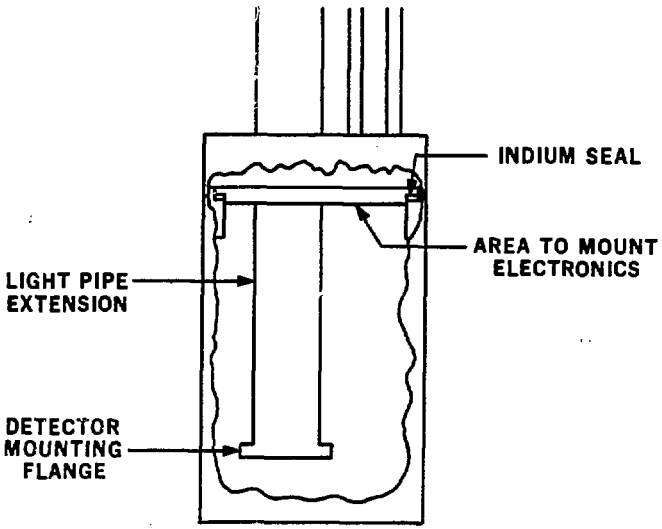

Figure 22. Cryostat sample chamber.

and at the top of the tubing carrying the electrical leads by a glass-to-metal feedthrough and Stycast. To perform low temperature measurements the insert was mounted at the top plate and hung down into an exisiting pyrex vessel into which liquid helium could be transferred using the provision made in the insert. The liquid helium vessel was surrounded by an insulating vacuum space which was in turn surrounded by a reservoir of insulating liquid nitrogen. The liquid helium vessel contained a port to facilitate pumping to achieve sub-4.2 K temperatures if desired.

D. JFET Testing.

Before an FET could be tested at low temperature, the process of eliminating unsuitable devices began with noise measurements at room temperature. The test circuit for these measurements is shown in

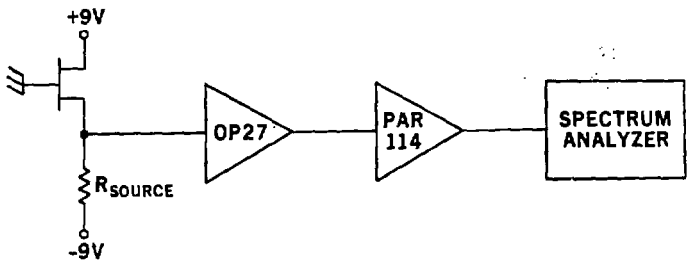

Figure 23. Test circuit for measuring voltage noise of JFETS.

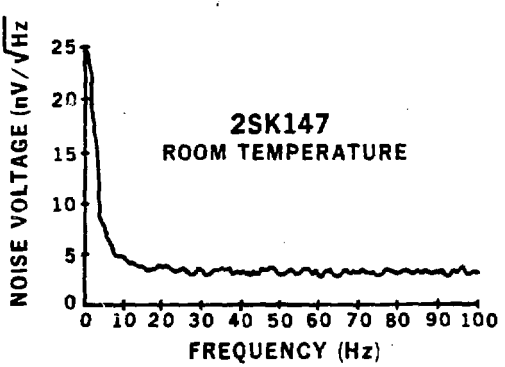

Figure 24. Noise spectrum of a Toshiba 2SK147 JFET.

figure 23. The noise voltage from the FET was displayed as a function of frequency using a Hewlett-Packard[43] spectrum analyzer as shown in figure 24. The sensitivity of the spectrum analyzer is limited to microvolts, thus the noise signal from the FET, in the range of nanovolts, was amplified in two stages. An ultra low noise Precision Monolithics[44] OP-27 operational amplifier was used to amplify the signal by a factor of ten and a PAR[45] 114 signal conditioning amplifier was

used for further amplification (10 - 100X) and for selection of bandwidth (generally 0.03 - 100 Hz). The total noise contribution of the amplifiers and spectrum analyzer are negligible compared to the FET and so did not affect the measurements. Several different types of FETs were tested with emphasis on the manufacturers who have been cited in the literature and the research community for production of devices which have proven successful in past applications. Since our interest was in the performance of these FETs at low frequencies and the noise in this 1/f range tends to vary from device to device of the same type, as many devices of the same type as could be practically secured were tested (generally in lots of 5 - 15 devices).

This process of elimination yielded two devices suitable for low temperature testing. First, however, an insulating housing had to be

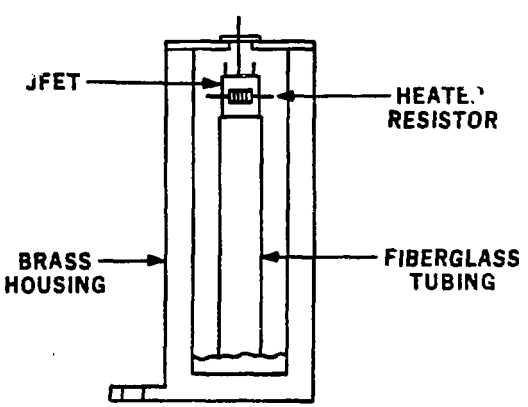

Figure 25. JFET insulating housing for mounting in cryostat sample chamber.

constructed to maintain the FET at an operational temperature in the 4.2 K environment. Shown in figure 25, the housing consisted of the FET epoxied on to a piece of 1 cm long, 1/8 in. diameter fiberglass tubing which was, in turn, epoxied into a hollow cylinder drilled out of a hexagonal brass rod. Epoxied on to the body of the transistor was a 1 kΩ carbon resistor to act as a heater. The source and drain leads from the FET as well as the heater resistor leads were soldered to four-pin feedthrough mounted on the side of the housing, while the gate lead was brought out through a feedthrough on the lid of the housing. A flange was soldered to the bottom of the housing for bolting to the inside of the cryostat sample chamber. Two such housings were constructed, one for a Siliconix[46] J230 and a second for a Toshiba[47] 2SK147. Both of these devices were then tested for noise in the cryostat sample chamber immersed in liquid helium. The circuit and amplification system was identical to that used at room temperature. Approximately 8 volts across the heater resistor was sufficient to keep the FET at an operating temperature.

E. Discussion of Results.

Table 3 shows the room temperature voltage noise measured at 10 Hz for the several FET types tested. In each case the value given repre-

TABLE 3. ROOM TEMPERATURE JFET VOLTAGE NOISE.

FET	VOLTAGE NOISE @ 10Hz ($nV/\sqrt{Hz}$)
2N4416	21.0
2N3875	17.6
TCG132	11.4
J230	7.3
2N4867	6.4
2SK147	4.4

sents the FET showing the best pe formance of the lot. The Toshiba 2SK147 measured the lowest noise with 4.4 nV/$\sqrt{Hz}$ followed by the Siliconix 2N4867 and J230 with 6.4 and 7.3 nV/$\sqrt{Hz}$, respectively. By virtue of these results, the 2SK147, 2N4867, and J230 were the only devices considered for low temperature testing. Chosen were the 2SK147 since it displayed the lowest value of voltage noise and the J230 also due to its low voltage noise at room temperature plus the fact that it had been used successfully in a similar application by Low.[48] The results for the two cooled transistors are given below in Table 4.

TABLE 4. VOLTAGE NOISE OF COOLED TRANSISTORS.

Device	Voltage noise (nV/$\sqrt{Hz}$) 10 Hz	5 Hz	2 Hz
J230	5.38	10.9	48.8
2SK147	6.00	28.8	109

In both devices an increase in the 1/f component at low temperatures caused an increase in the measured noise at 10 Hz and below for the 2SK147 and at 5 Hz and below for the J230. It is not clear why cooling the FET in this housing should increase the 1/f noise. One hypothesis, however, is that temperature fluctuations occur within the device which transform into an 1/f noise characteristic. This effect has been noted in bolometers and resistors at low temperatures in thermally unstable liquid helium baths.[49] Nevertheless, the performance of the J230 is acceptable for use in bolometer circuits for sampling frequencies of 5 Hz and greater and provides the necessary impedance lowering to avoid microphonic problems. The use of this device at lower frequencies is dependent upon the sensitivity required by the specific application. This particular device will be used in future

work involving bolometer noise and responsivity measurements.

V. SUMMARY AND CONCLUSIONS.

1. The behavior of defects generated during the neutron-transmutation-doping of germanium was studied using deep level transient spectroscopy. Hole traps located at 0.10, 0.14, 0.22, 0.027, and 0.37 eV above the valence band were detected. Thermal annealing at 400°C for six hours is sufficient to annihilate each of these deep levels. Traps H(0.10), H(0.22), and H(0.37) exhibited the Poole-Frenkel effect and determined to be acceptors. Recombination enhanced annealing, alone and in conjunction with thermal annealing was used to repair deep level damage within the diffusion length of electrons across the forward biased junction.

2. DLTS was used to monitor the increased electrical activity of deep selenium donors with annealing time at 400°C. Even in unannealed material, variable temperature Hall effect revealed approximately one half of the calculated number of donors were already electrically active.

3. A semi-automated process of attaching electrical leads on to 0.5 x 0.5 x 0.3 mm^3 germanium chips for the fabrication of bolometers was developed. The chip is heated by a Kovar strip heater while wires tinned with fluxed indium solder balls are positioned with micro-manipulators to make the bond. In addition, a new contact metallization scheme consisting of a 200 Å layer of palladium and an 8000 Å layer of gold on germanium was developed to improve the adhesion characteristics of the previously used titanium-gold system. Upon stress relief annealing, the palladium forms an intermetallic compound, probably PdGe, at the metal-semiconductor interface, thus inhibiting the flaking of the metallization.

4. Several different types of junction FETs were measured for voltage noise at room temperature. Of these, the Siliconix J230 and 2N4867 and the Toshiba 2SK147 were judged best suited for testing at low temperatures and possible use as first stage bolometer amplifiers. An insulating housing was constructed for measuring the voltage noise of the J230 and 2SK147 at low temperatures. The J230 and the 2SK147 measured 5.38 and 6.00 $nV/\sqrt{Hz}$ at 10 Hz and T ~ 80 K with increasing noise at lower frequencies. The J230 will be used in future bolometer characterization experiments.

Neutron-transmutation-doped germanium is well suited for application as low temperature bolometer material. The ability to cover a large doping range by simply specifying the neutron dose makes available to the bolometer designer material of optimum resistivity over a wide range of operating temperatures. This study has answered questions concerning the proper annealing procedures for NTD germanium as well as described a method to successfully fabricate bolometers out of small chips of NTD germanium. This information along with the development of a low noise amplification system will lead to future performance testing and operation of NTD germanium bolometers in a variety of infrared experiments. In addition to bolometer optimization, future work in NTD germanium will involve accurate determination of the neutron capture cross-section as a function of neutron energy, additional irradiations and low temperature resistivity measurements to further fine tune the available material for specific temperature applications, and applications of NTD germanium as very accurate low temperature thermometers in cryogenic equipment. One of the most ex-

citing aspects will be the lowering of the operating temperature to below 100 mK. Bolometer performance estimates show that NEP limits as low as the numbers achieved by photoconductors should be achievable. The engineering of such low temperature detector systems for space flight applications is a great challenge and is presently pursued by a number of groups.

VI. APPENDIX

Bolometer operation may be understood by first studying the thermal equivalent circuit and setting up a power balance. As shown in figure 2 the absorbed power in the bolometer, ηP, can be accounted for as the sum of the heat used to warm the detector plus the heat conducted to thermal sink,

$$\eta P = H(d\theta/dt) + G\theta$$

η = absorption efficiency
P = incident power
H = thermal mass
θ = temperature increase above sink temperature
t = time
G = thermal conductance to sink

At low temperatures the power dissipated by the device due to radiation can be ignored. The incident power may be divideo into a constant background, P_0, and a time varying signal:

$$P_s = A\exp(i\omega t)$$

Substituting this into the power balance and solving for θ_s gives,

$$\theta_s = \eta A(G^2 + \omega^2 H^2)\ \exp(i\omega t + \Psi)$$

with phase shift:

$$\Psi = \arctan(\omega H/G)$$

The response time of the device, τ, is simply the ratio of thermal mass to thermal conductance,

$$\tau = H/G$$

From this derivation, some insight may be obtained surrounding some of the parameters which may be manipulated during bolometer design and construction. For instance, the signal temperature fluctuation may be maximized by minimizing the thermal mass, H (by using low heat capa-

city material, low temperature operation, using the smallest possible device). In addition, the response time may be varied by choosing the thermal link to the heat sink (pure metal wire for small time constant, alloy wire for long time constant).

The transformation from temperature fluctuation to elecrical signal may be understood by studying the electrical circuit of figure 1. A constant current, I, biases the detector producing a voltage drop across the bolometer resistance. As the temperature of the device fluctuates so does its resistance, producing a corresponding signal voltage V_s. A capacitor filters out the DC voltage drop from the signal portion. The temperature coefficient of resistance is

$$\alpha = R^{-1}(dR/dT)$$

and can be used in the expression for V_s,

$$V_s = I\alpha Re_s$$
$$= I\alpha R\eta P_s(G^2 + \omega^2 H^2)$$

The responsisity, S, in volts per watt is then

$$S = V_s/P_s = \eta I\alpha R(G^2 + \omega^2 H^2)$$

The current and resistance in the expression are intimately related through the Joule heating of the detector which acts as an additional source of power not included in the analysis. This self-heating of the device results in a highly non-linear dark bolometer I-V curve. The maximum responsivity with respect to current occurs at the operating point where this curve displays a maximum in non-linearity.

VII. REFERENCES

1. S. P. Langley, Nature 25, 14 (1881).

2. J. C. Mather, SPIE 280, (1981).

3. E. H. Putley, Topics in Applied Physics vol. 19, R.J. Keyes, ed., Springer-Verlag, New York (1980).

4. J. Clarke, G. I. Hoffer, P. L. Richards, and N. H. Yeh, J. Appl. Phys. 48, 4865 (1978).

5. F. J. Low, J. Opt. Soc. Amer. 51, 1300 (1961).

6. N. S. Nishioka, P. L. Richards, and D. P. Woody, Appl. Opt. 17, 1562 (1978).

7. C. Kittel, Introduction to Solid State Physics, 5th ed., John Wiley and Sons, New York (1976).

8. K. F. Berggren, Phys. Rev. 17, 2631 (1978).

9. G. Chanin, Infrared Detection Techniques for Space Research, V. Manno and J. Ring, eds., D. Reidel Publ. Co., Dordrecht, (1972).

10. M. A. Kinch, J. Appl. Phys. 42, 5861 (1971).

11. P. M. Downey, Ph.D. Thesis, Dept. of Physics, Massachusetts Institute of Technology (1980).

12. W. Keller and A. Muhlbauer, Floating Zone Silicon, Marcel Dekker, Inc., (1981).

13. H. Fritzsche and M. Cuevas, Phys. Rev. 119, 1238 (1960).

14. H. M. Janus, Neutron Transmutation Doping in Semiconductors, J. M. Meese, ed., p. 37, Plenum Press, New York (1979).

15. M. Rodder, Master's Thesis, Dept. of Materials Science, Univ. of California, Berkeley (1982).

16. H. J. Stein, ref. 14, p. 229.

17. J. M. Meese, M Chandrasekar, D. L. Cowan, S. L. Chang, H Yousif, H. R. Chandrasekar, and P McGrail, Neutron Transumtation Doped Silicon, J. Guldberg, ed., p. 101, Plenum Press, New York (1981).

18. J. W. Cleland, P. H. Fleming, R. D. Westbrook, R. F. Wood, and R. T. Young, ref. 14, p.261.

19. K. Kuriyama, M. Yahagi, K. Iwamura, Y. Kim, and C. Kim, J. Appl. Phys. 54, 673 (1983).

20. D. V. Lang, J. Appl. Phys. 45, 3014 (1974).

21. G. L. ..ller, J. V. Ramirez, and D. A. H. Robinson, J. Appl. Phys. 46, 2638 (1975).

22. L. C. Kimerling and J. L. Benton, Appl. Phys. Lett. 39, 410 (1981).

23. L. C. Kimerling and D. V. Lang, Inst. Phys. Conf. Series 23, 589 (1975).

24. D. V. Lang, R. A. Logan, and L. C. Kimerling, Proc. XIII Intl. Conf. Physics of Semiconductors, Rome, p. 615 (1976).

25. N. Fukuoka and H. Saito, Jap. J. Appl. Phys. 21, 930 (1982).

26. S. J. Pearton, A. J. Tavendale, J. M. Kahn, and E. E. Haller (unpublished).

27. J. M. Meese, University of Missouri Research Reactor Facility.

28. L. J. van der Pauw, Philips Res. Repts. 13, 1 (1958).

29. J. Frenkel, Phys. Rev. 54, 647 (1938).

30. A. O. Evwaraye, R. N. Hall, and T. J. Soltys, IEEE Trans. on Nucl. Sci. NS-26, 271 (1979).

31. A. Seeger, H. Foll, and W. Frank, Inst. of Phys. Conf. Series 31, 12 (1977).

32. L. C. Kimerling, Physica 116B, 1 (1983).

33. M. Hirata and M. Kiritani, Physica 116B, 623 (1983).

34. H. Saito, N. Fukuoka, and H. Yoshida, Inst. Phys. Conf. Series 59, 45 (1980).

35. T. V. Mashovets and V. V. Emtsev, Inst. Phys. Conf. Series 23, 103 (1975).

36. S. J. Pearton, N. P. Palaio, and E. E. Haller, to be published.

37. NASA Progress Reports, Contract W-14,606.

38. P. Luke, Dept. of Eng. and Tech. Services, Lawrence Berkeley Laboratory, Univ. of California, Berkeley, private communication.

39. D. N. B. Hall, R. S. Aikens, R. R. Joyce, T. W. McCurnin, Appl. Opt. 14, 450 (1975).

40. Siliconix Small Signal FET Design Catalog, November 1982.

41. P. L. Richards, Dept. of Physics and Lawrence Berkeley Laboratory, Univ. of California, Berkeley.

42. Stycast 2850-FT, Emerson and Cuming, Inc., Gardena, CA.

43. Hewlett-Packard Co., Loveland, CO 80537.

44. Precision Monolithics, Santa Clara, CA 95050.

45. Princeton Applied Research Corp., Princeton, NJ 08540.

46. Silicoix Inc., Santa Clara, Ca. 95054.

47. Toshiba America Inc., Tustin, Cal 92680.

48. F. J. Low, Steward Observatory, Univ. of Arizona.

49. A. Lange, Dept. of Physics, Univ. of California, Berkeley, private communication.